Revista Facultad de Ingeniería Universidad de Antioquia
ISSN: 0120-6230
revista.ingenieria@udea.edu.co
Universidad de Antioquia
Colombia

Urquijo, Jeaneth Patricia; Casanova, Herley; Morales, Alvaro L.; Zysler, Roberto D.
Engineering iron oxide nanoparticles for biomedicine and bioengineering applications
Revista Facultad de Ingeniería Universidad de Antioquia, núm. 71, junio-, 2014, pp. 230-243
Universidad de Antioquia
Medellín, Colombia

Engineering iron oxide nanoparticles for biomedicine and bioengineering applications

Diseño de nanopartículas magnéticas para aplicaciones en biomedicina y bioingeniería

Jeaneth Patricia Urquijo[1,2], Herley Casanova[2], Alvaro L. Morales[1], Roberto D. zysler[3]*

[1]Grupo de Estado Sólido, Instituto de Física, Facultad de Ciencias Exactas y Naturales, Universidad de Antioquia.Calle 70 Nº. 52-21. AA. 1226. Medellín, Colombia.

[2]Grupo de Coloides, Instituto de Química, Facultad de Ciencias Exactas y Naturales, Universidad de Antioquia. Calle 70 Nº. 52-21. AA. 1226. Medellín, Colombia.

[3]Centro Atómico Bariloche / CONICET. CP. 8400. S.C. de Bariloche, Argentina.

(Recibido el 19 de junio de 2013. Aceptado el 19 de febrero de 2014)

Abstract

In the present study the one-step coprecipitation method is used to obtain magnetic nanoparticles at controlled pH of 10 and 12, and surfactant concentration of 1% and 3%(m/m). The surfactant is sodium polyacrylate(PS), biocompatible and biodegradable, necessary attributes for biological applications. The magnetic nanoparticles have a magnetite core, and a shell of maghemite surrounded by a shell of polymer. The maghemite layer is smaller for large surfactant concentration(3%) and pH 10. The TEM images confirm the particle size distribution in the average range of 5-10 nm. Mössbauer results at 80 K showed line shapes dominated by magnetic relaxation effects with sextets and combinations of sextets and doublets for pH 12. The doublet features dominated the samples obtained at pH 10.

The interactions of the surfactant with the nanoparticle surface, mainly with the Fe^{3+}, is strong showing at least two surfactant layers, one layer directly over the nanoparticle surface and another layer resting over the inner layer. FTIR confirmed the attachment of the surfactant to the magnetic nanoparticle surface. The nanoparticles showed superparamagnetic behavior at room temperature and ferromagnetic properties at 5 K. The saturation magnetization presented lower values than reported bulk systems due to the presence of a

* Autor de correspondencia: teléfono: + 57 + 4 + 219 5630, correo electrónico: amoral@fisica.udea.edu.co (A. Morales)

large layer of maghemite. The very close particle size for all samples gave indication that the particle growth was dominated by the surface properties of the nanoparticles and that the pH and surfactant concentration did not affect importantly the growth process.

----------*Keywords:* Magnetic nanoparticles, sodiumpolyacrylate, Mössbauer spectroscopy, thermo magnetic measurements, FTIR, TEM

Resumen

Se usó el método de coprecipitación en un solo paso controlando el pH a 10 y 12 y en concentraciones de poliacrilato(PS) de 1% y 3%(m/m). El surfactante es biocompatible y biodegradable, atributos necesarios para su uso en aplicaciones biológicas. Las nanopartículas magnéticas están formadas por una coraza interna de magnetita, una capa de maghemita y una capa externa del polímero. La capa de maghemita es pequeña para la concentración de 3% y pH 10. Las imágenes de TEM confirman la distribución de tamaños de partícula en el rango promedio de 5-10 nm. Los resultados Mössbauer a 80 K mostraron formas de línea dominadas por efectos de relajación magnética en forma de sextetos y combinanciones de sextetos y dobletes; estos dominaron a pH 10. Las interacciones del polímero con la superficie de las nanopartículas, principalmente con el Fe^{3+}, es fuerte mostrando al menos dos capas del polímero sobre ellas. Las medidas magnéticas muestran un comportamiento superparamagnético a temperatura ambiente y ferrimagnético a 5 k. La magnetización de saturación presentó valores menores que las repotadas para volúmenes grandes debido a la caapa de maghemita presente. El tamaño de partícula obtenido para todas las muestras es muy cercano entre si indicando que el crecimiento de las partículas fue dominado por las propiedades de la superficie de estas y en menor grado por las condiciones de concentración y pH usadas.

----------*Palabras clave:* Nanopartículas magnéticas, poliacrilato de sodio, espectroscopia Mössbauer, medidas magnética térmicas

Introduction

Magnetic nanoparticles, covered with polymers, based on iron oxides, particularly mixtures of magnetite and maghemite, have been synthesized by different routes, coprecipitation, sol-gel, ionic liquids, etc, for more than one decade [1-3], in order to acquire enough knowledge to apply them in industry and biomedicine [4]. The colloidal stability is of primary importance to ensure the proper performance of the ferrofluids and also the further functionalization of the physical-chemical system. Issues about biocompatibility and biodegradability have been also addressed in order to use this systems in biology and medicine.

Researchers in [3] have synthetized magnetite, in acrylic acid anion at concentrations smaller than 0.5%(m/m), obtaining sizes between 12-20 nm and confirming by FTIR and TGA that the anion has been attached to the surface in a chelating bidentate configuration. Authors in [5] obtained almost spherical 5.5 nm diameter magnetite particles from a sol-gel method. The nanoparticles were covered with two substances oleic and dodecanoic acids with a concentration

of magnetite in the range 63-78% and saturation magnetization ranging from 83,2-96,0 emu/g. these high values are explained as an effect of the acids preventing surface spin disorder. Also, due to their high magnetite concentration they found that interparticle dipolar interactions were important.

Further research by authors in [6] obtained poly(methyl methacrylate) or polystyrene/ magnetite nanocomposites, the polymers were added after the magnetic particles were formed. For the 32% wt and 6%wt iron oxide samples the saturation magnetization was 13 and 3 emu/g and coercitivity 240 and 220 Oe respectively. The particles showed a cubic morphology with 20 nm average size. In [7] it was prepared stable magnetite-copolymer complexes with magnetite percentage running from 6.9% to 45.5 % wt. They obtained first the 9 nm nanoparticles and afterwards they were coated with the copolymer, two-step process, by an elaborate technique, being able to control its amount. Saturation magnetization were in the range 67-75 emu/g and carboxylic acid groups were the dominant binding mechanism to the particle surface.

Studies in [8] have simulated theoretically the interparticle interactions in field cooling(FC) measurements and they found a flattening of the FC curve at low temperatures as a signal of such interactions, for monodisperse particles, or weak interacting particles, the FC curve increases monotonically as the temperature decreases. They also produce 4 nm average maghemite nanoparticles by microwave plasma method and from them obtained monodisperse and compacted samples for which the FC experimental curves were in agreement with the computer simulations.

Tetramethyl ammonium hydroxide (TMAOH)-functionalized 8 nm nanoparticles were obtained in [9] using the one-step coprecipitation method. They found, by oxidizing the nanoparticles to drive the transformation from magnetite to maghemite, a decrease in the saturation magnetization and this effect also helped to improve colloidal stability because magnetic interaction between them decreased. In reference [10], researchers have tested the adsorption behaviour and wettability of synthetic magnetite and mineral particles. They obtained iron oxide nanoparticles by a two step route where in the first step they used a primary surfactant and sodium polyacrylate (PS) was used as a second layer surfactant at pH 8.5. The primary surfactant helped the adsorption of PS by reducing the electrostatic repulsion between the particles and PS. Their results indicate that the wettability of both synthetic magnetite coated with a primary surfactant and magnetite mineral can be improved by adsorbing a hydrophilizing agent such as polyacrylate.

In the present study the one-step coprecipitation method is used to obtain magnetic nanoparticles at controlled pH of 10 and 12, and surfactant concentrations of 1%(m/m) and 3%(m/m). The surfactant was sodium polyacrylate. PS is an anionic polymer, with negative charge carboxylic groups, with a uniform distribution of ionizable groups along its chain and highly soluble in water, it is also biodegradable and biocompatible. The PS has been used generally as a secondary cover on magnetic nanoparticles, here it is used as the first layer on them. PS provide the required electrosteric properties to stabilize the nanoparticle fluid, at the same time the surfactant adhere to the nanoparticle surface providing a way to further functionalize the system. Furthermore, the surfactant is intended as a mean of controlling the nanoparticle growth.

Experimental

The magnetic nanoparticles were obtained by the coprecipitation method [11], with appropriate modifications, starting with precursors $FeCl_3.6H_2O$ (≥99.0%), $FeCl_2.4H_2O$ (≥99%) y NaOH (≥99%), obtained from Merck®, and sodium polyacrylate commercial grade. All solutions were prepared and the synthesis ran under nitrogen flux in order to avoid oxidation. Also, deionized water was used in the solution preparation. A 0.06 M solution of Fe^{2+}, a 0.12 M solution of Fe^{3+}, and a 2M solution of NaOH were poured into a solution

of the surfactant with automatic pH control using a Metrohm 907. Magnetic stirring of the solution was kept during all the synthesis time at room temperature 21-23 C.

The black product was washed using a dialysis membrane until the conductivity of the water was the same as the conductivity of deionized water. The nanoparticles embedded in the polymer were dried using mechanical vacuum, a part of the solutions were converted to gel, by adding 0.2g/ml agar per ml of magnetic solution, to preserve the particle distribution in the fluid. The same synthesis was repeated without the surfactant to obtain a set of nanoparticles as a reference (Pph12, Pph10). The synthesis was carried out for pH of 10 and 12 and surfactant concentrations of 1% and 3% (m/m), the samples were named as concentration-surfactant-pH, e.g. 1PS12, etc. In order to assess the amount of iron in the samples, i.e. the amount of magnetite/maghemite, Atomic absorption spectroscopy (AAS) was used.

To corroborate the phase composition, magnetite and maghemite, of the product obtained Microraman (MR) measurements were taken in a Horiba Jobin Yvon, model Labram HR, with CCD detector with resolution of 1024x256 pixels, spectral range of 100-500 cm^{-1} and a 633 nm He/Ne laser. The crystalline structure of the spinel phases was probed by X-ray diffractograms taken with CuKα radiation in the range 10-80 2θ, step 0.02 2θ, 3 seconds per step. The XRD analysis was performed with program powderx [12] and observed peaks were assigned according to the JCPDS cards [13].

The morphology and particle size distribution were investigated by transmission electron microscopy(TEM) with a Philips CM200 UT microscope, operating at 200 kV. Magnetic information on the samples was obtained by means of the Mössbauer technique in a Wissel spectrometer with MR-260 transducer, ^{57}Co (Rh) source, and a closed-cycle cryostat, the hyperfine parameters were extracted by program DISTRI [14]. All spectra were fitted with hyperfine field and quadrupole splitting distributions due to the asymmetric line shape found. The sextet spectra for the pH 12 samples were fitted using a modification of the model by Berry et al. cited in [15] which consist of five iron sites, Fe^{3+} (F3T)from tetrahedral sites, Fe^{3+} (F3O)from octahedral sites, a mixed-valence $Fe^{2.75+}$ (F32O)from octahedral sites, Fe^{2+} (F2O)from octahedral sites, and a Fe^{3+} (F3S)sextet coming from the surface of the particles. This site was included because the spectra showed a feature different from the spectra reported in [15].

The interaction of the surfactant with the surface of the nanoparticles was sensed by both Fourier Transform Infrared Spectroscopy, in a Perkin Elmer equipment, and thermogravimetic analysis, in a T.A Instruments Q100 v. 9.9. Further, magnetic characteristics of the samples were analyzed by magnetic field versus magnetic moment measurements in a Quantum Design PPMS, Vibrating Sample Magnetometer, in the temperature range 5-300 K.

Results and discussions

Information on the crystalline structure, morphology and composition of the nanoparticles were obtained from XRD, fig. 1, MR, fig. 2, and TEM, fig. 3.

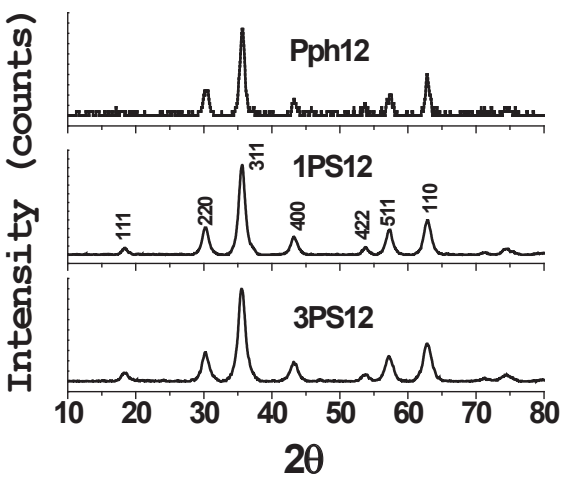

Figure 1 X-ray diffraction spectra for samples 1PS12, 3PS12, Pph12 showing only spinel peaks belonging to magnetite and maghemite. Diffraction planes are specified

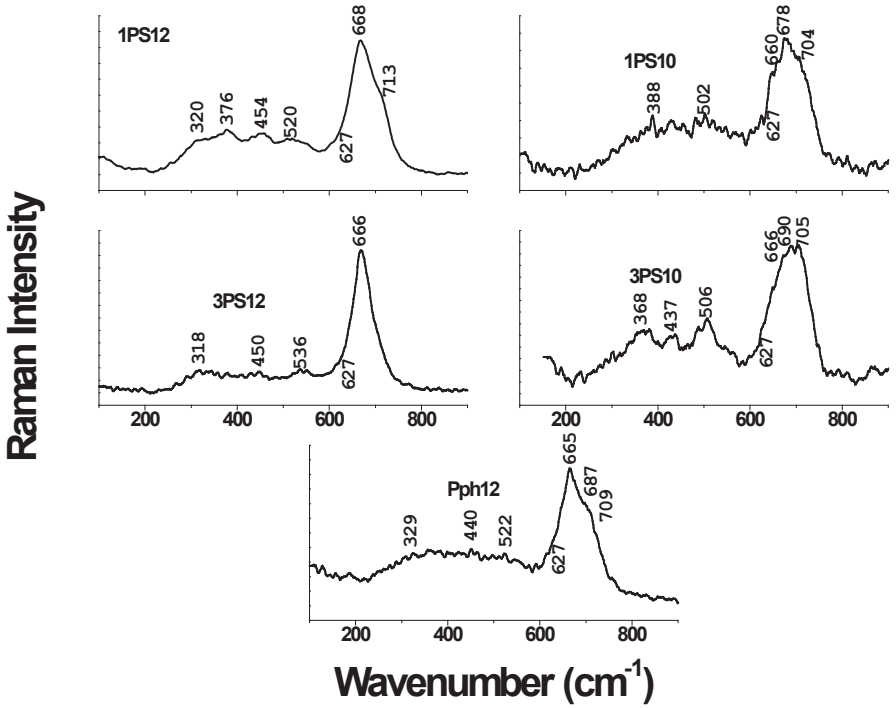

Figure 2 Raman spectra for samples taken at pH 10 and 12 and a pure sample Pph12. Peaks correspond to magnetite and maghemite phases

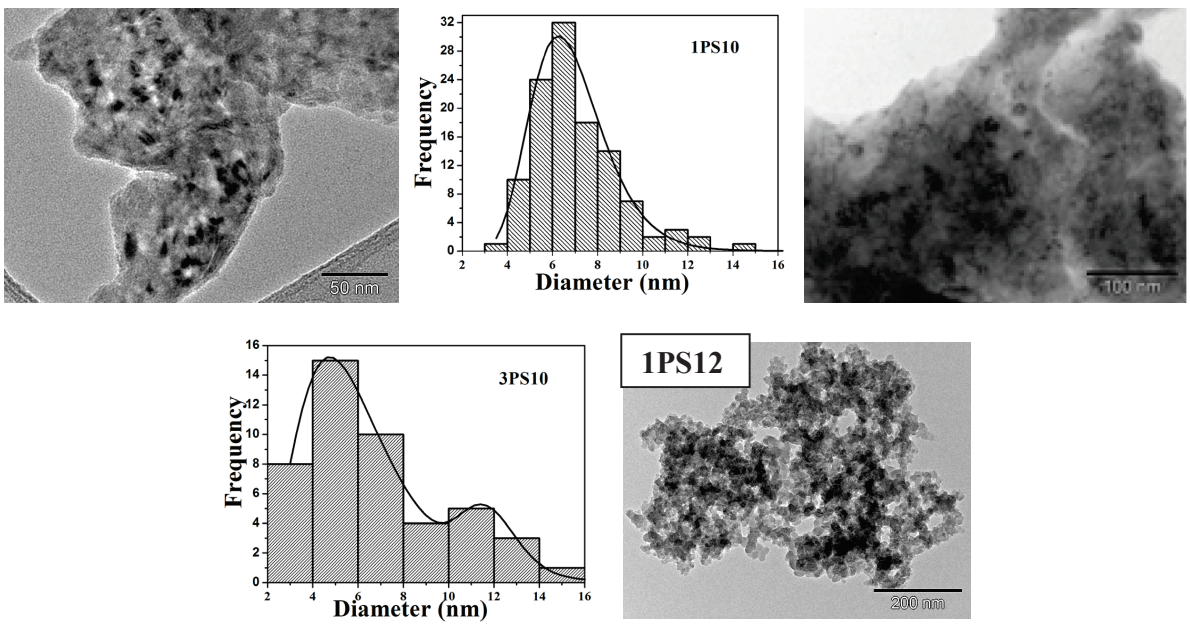

Figure 3 TEM micrographs for selected samples obtained at pH 12 and 10 and their particle distribution. The particles are embedded in the polymer host 1PS10 upper left, 3PS10 upper right

XRD shows spinel peaks, belonging to both magnetite and maghemite not separable by this technique. The peaks are broad due to the small particle size of the samples, this broadening leads to crystallite sizes, by using the Scherrer's formula with an error of 10%, of 10 nm and 9 nm for 1PS12 y 3 PS12 samples respectively.

MR results shows that the nanoparticles were formed as a mixture of magnetite and maghemite, and they suffered further oxidation due to the drying process. The assignment of strongest peak positions for all samples was based on the literature [16]. The uncovered sample (Pph12) shows a similar spectra with peaks corresponding to magnetite and maghemite. The main structure around 600-800 cm^{-1} is broad due to particle size distribution in the samples and to overlapping phases, and it consist of three peaks at around 665 cm^{-1}, 680 cm^{-1} and 709 cm^{-1}. The first peak corresponds to magnetite, the third peak has been assigned in [16] to iron oxidation at the magnetite B-sites, i.e. non-stoichiometric magnetite, but other authors assigned it to maghemite [17]. The peak at 680 cm^{-1} has not been reported in the literature as a peak belonging to magnetite or maghemite but it may come from the interface separating the magnetite core from the maghemite layer. Peaks around 374 cm^{-1} and 627 cm^{-1} belong to maghemite.

The similar Raman spectra for plain and covered spectra points to the fact that the dominant oxidation process is during the drying stage. The MR spectra of pH 10 samples showed more noisy spectra due to the larger amount of polymer covering the particles. The amount of polymer stuck to the surface of the particles was evaluated by AAS. The amount of magnetite in the dry samples was, for pH 12 samples 93.5(1%) and 83.1(3%) and for pH 10 samples 49.8(1%) and 15.3(3%). As a result, the amount of polymer decreases in the order 3PS10, 1PS10, 3PS12, 1PS12. The amount of surfactant deposited on the particles can be understood considering the negatively charge increase on the particle surface and on the polymer surface as the pH increases leading to a larger electrostatic repulsion. Both surfaces, iron oxide and polymer, are negatively charged since they are well above the zero charge point (ZCP). Researchers in [18] had reported a 95% polymer ionization at pH 8.

Of course, additional binding mechanisms are acting in those systems like steric repulsion, Van der Waals forces, surface complexation and formation of hydrogen bridges. The layers over the nanoparticles will play an important role for applications since functionalizing substances can be added on them.

TEM adds information on the morphology, particle size and its distribution. Figure 3 shows the outcome for selected samples. All micrographs show the nanoparticles embedded in the respective polymer which makes difficult the assessment of the morphology, i.e. the particle size and its distribution. The main features present in the micrographs are isolated nanoparticles of irregular form, aggregated particles, and polymer surrounding the particles. Nevertheless, the analysis was performed to obtain the particle size distribution and average size of the nanoparticles. The frequency plot for the particle size, only isolated particles were taken into account, 46 particles for 3PS10 and 114 for 1PS10, was adjusted to a log-normal distribution [19] in this way the average particle size and standard deviation were obtained. A systematic error comes from the blurring of the images due to the polymeric layer on the particles making the results for the averages just approximate. Average sizes are 6 ± 2 nm for 1PS10, 5 ± 2 nm for 3PS10. These averages are essentially the same indicating that at these high concentrations the particle size comes out nearly the same in spite of the fact that the surfactant concentration is rather different. These sizes are in agreement with the crystallite size given by XRD (see below a comparison of crystallite sizes).

The magnetic properties of the nanoparticles were investigated by MS, fig. 4, Hysteresis measurements, fig. 5, and FC/ZFC measurements, fig. 6.

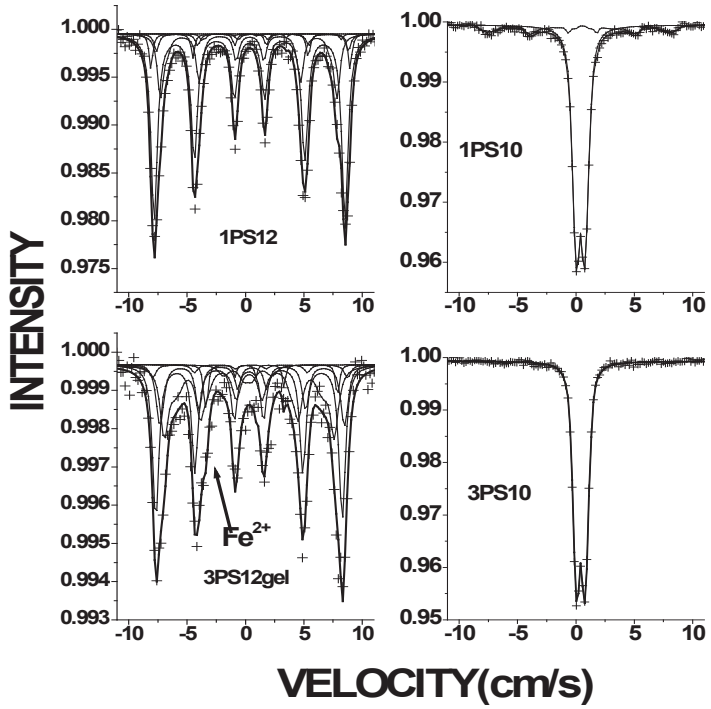

Figure 4 80 K Mössbauer spectra for selected powder samples. Sample 3PS12gel was taken in gel form to clarify the presence of Fe^{2+}

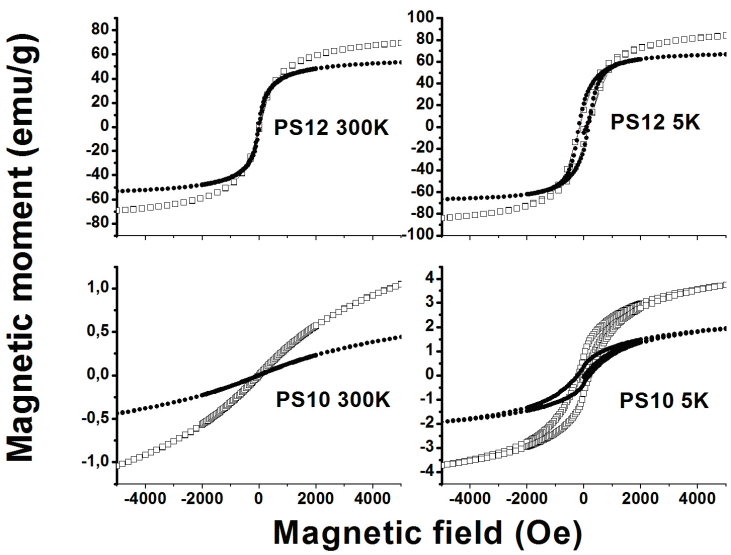

Figure 5 Hysteresis loops for all samples taken at 300 K, presenting paramagnetic behavior, and 5 K, presenting ferrimagnetic behaviour. Open squares represent 1% concentration and solid dots 3% concentration

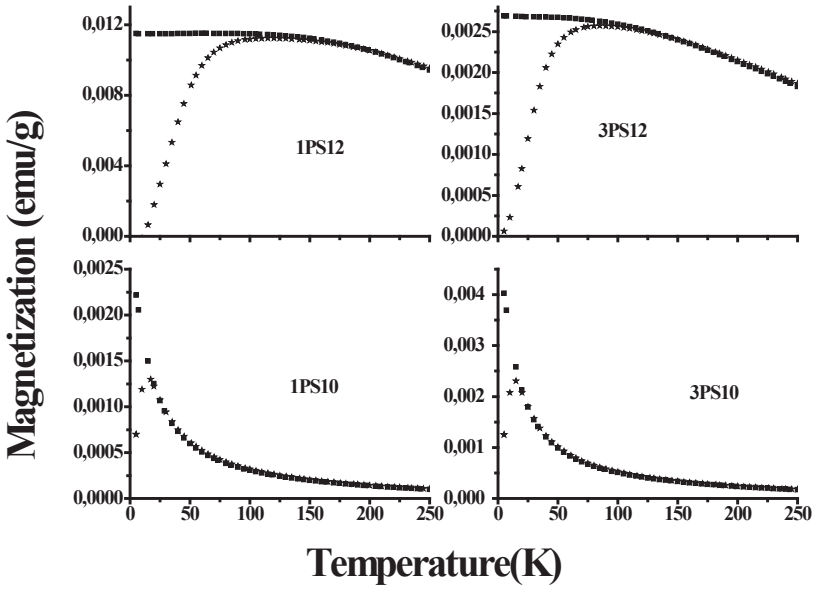

Figure 6 FC(squares) and ZFC(stars) plots for the samples showing strong interparticle interactions for pH 12 and weak interactions for pH 10

The Mössbauer hyperfine parameters, for dry samples, at 80 K are shown in Table 1. The spectra are composed of sextets for samples obtained at pH 12, a very small doublet is present. The sextets show dominant components of Fe^{3+} and smaller components of mixed valence $Fe^{2.75+}$ (IS=0.54-0.74 mm/s). The fact that these sites are present tells that the samples are ferrimagnetic at this temperature, they present the Verwey transition at 125 K, and present good crystallinity. The sextets are dominated by magnetic relaxation effects due to the broader and asymmetric lines; this is related to the small particle size and its distribution.

Table 1 Hyperfine parameters for samples at 80 K

Sample	*Site*	*IS (mm/s) ±0.02*	*ΔQ (mm/s) ±0.02*	*B Average (T) ±0.01*	*B Maximun (T) ±0.01*	*Area(%) ±4*
1PS12	F3T	0.46	0.01	50.69	50.68	64
	F3O	0.74	-0.07	50.97	50.92	5
	F32O	0.54	0.00	52.91	52.84	8
	F3S	0.44	-0.10	46.28	47.04	23
3PS12	F3T	0.41	0.01	49.87	49.25	24
	F3O	0.64	-0.07	53.27	53.49	17
	F32O	0.69	0.00	49.12	49.14	14
	F3S	0.44	0.01	42.83	45.14	40
	Doublet	0.31	0.66			5
1PS10	Sextet	0.53	-0.29	40.06	48.65	15
	Doublet	0.51	0.56			85
3PS10	Doublet	0.53	0.84			100

(continue)

Table 1 Continue

Sample	Site	IS (mm/s) ±0.02	ΔQ (mm/s) ±0.02	B Average (T) ±0.01	B Maximun (T) ±0.01	Area(%) ±4
3PS12g	F3T	0.41	0.01	49.50	49.15	39
	F3O	0.54	-0.07	51.72	51.91	3
	F2O	1.21	2.20	35.27	35.33	4
	F32O	0.69	0.00	48.95	48.77	17
	F3S	0.44	0.01	43.26	45.30	33
	Doublet	0.31	0.62			4

For the sample 1PS10 a superparamagnetic doublet dominates the spectrum and a small magnetic component exist. For the sample with 3% surfactant concentration and pH 10, it can be noticed a pure doublet with two clear peaks. It must be emphasized that the Mossbauer spectra line shape could be affected by interparticle interactions, due to the particle density in the polymer as shown by AAS, i.e. for the highest particle densities sextets are found and for the lower ones superparamagnetic doublets and small magnetic components are observed.

These results mean that although the particles are small in size or superparamagnetic, recall the Scherrer's crystallite size, due to the relative closeness at high particle densities they interact and produce a magnetic signal. As a consequence, the Mossbauer line shape is attributed mainly to the presence of interparticle interactions and not to a large size magnetic particles in agreement with [20]. In general, for large iron oxide particles, the crystallite size derived from XRD is smaller than the size given by TEM so the particles are polycrystalline [21]. The general trend showed by the Mossbauer spectra is that for pH 12 samples the spectra showed magnetic components, and for the pH 10 samples superparamagnetic behavior dominated; this trend point to the presence of particles of nanometer size. Since the sextets showed mainly Fe^{3+} components a different way of preparing the sample was tried, i.e. instead of drying the sample it was converted to a gel to preserve the original phase composition of the nanoparticles. The result is showed in Fig. 4 for the sample 3PS12g where the Fe^{2+} peak is reveled. In this way the presence of magnetite was further confirmed and the oxidation effect on the samples during the drying process. Next, the magnetic behavior of the nanoparticles was analyzed by hysteresis measurements, figure 5 and table 2 [22-25].

Table 2 Magnetic parameters for the samples

	5K		300K		
Sample	Ms (emu/g)	Hc(Oe) ± 10 [25]	Ms (emu/g)	Hc(Oe) ± 10 [25]	χi
Magnetite	96 [24]	784 [23]	85-100 [22]	115-150 [22]	
Maghemite	87 [24]		74 [24]		
Pph10	75.86	323	70.17	13	
1PS12	84.11	156	69.61	20	0.0669
1PS10	3.77	191	1.06	14	0.0161
3PS12	66.61	197	53.53	24	0.1011
3PS10	1.94	205	0.45	14	0.0064

It is important to remember that the samples were prepared as gels to keep the particle distribution in the fluid, this will influence the results and they may be different from some of the results shown above for powder samples for which an extra oxidation took place. The main characteristic at 300 K was the superparamagnetic behavior of the samples in contrast to 5 k where they behaved as ferrimagnetic. The small coercive fields, measured at room temperature, are probably due to a tiny magnetic component coming from aggregation of particles and a small number of large particles. The magnetic saturation is the largest for 1PS12 and decreases for 3PS12, but for the pH 10 samples the magnetic saturation is very small. The magnetic saturation is considerable smaller than reported bulk values. The coercive field for bulk samples is not comparable with its counterpart for nanoparticles because they come from different physical mechanisms; for the bulk it is a consequence of the pinning of domain walls while for the nanoparticles it comes from the anisotropy energy barriers. These smaller magnetic saturations as compared with reported values ([5, 7]) are due to the maghemite layer surrounding the magnetite core in agreement with [9].

At 5 K the samples behaved as ferrimagnetic showing large values of the susceptibility and the coercive fields. From the measured initial susceptibility an estimation of the magnetic particle size, corresponding to the largest particles present in the distribution, can be made using the formula, $d^3_{mag} = {}^{18K_B T\chi_i}/_{(\mu\pi_0 M_s M_B)}$, where K_B, T, χ_i, μ_0, M_s, M_B, stand for the Boltzmann constant, temperature, initial susceptibility, vacuum permeability, saturation magnetization for nanoparticles, saturation magnetization for bulk magnetite. The magnetic particle size is presented in table 3 from which it can be deduce that the particle size obtained from these samples is very similar in spite of the fact that the surfactant concentrations are very different.

Table 3 particle sizes by different techniques

sample	*TEM(nm)*	*XRD (nm)*	*d_{mag}(nm)*
1 PS-12 a 1PS12		10	6
3 PS-12 a 3PS12		9	8
1 PS-10 a 1PS10	6		15
3 PS-12 a 3PS10	5		15

This result indicates that it is the surface properties of the nanoparticles the dominant fact by which the surfactants bind to it, in this way the chelanting mechanism by which the surfactants stick to the Fe^{3+} sites is confirmed. For this kind of superparamagnetic particles the sizes given by XRD, TEM, and magnetic measurements are very close to each other [26].

The FC/ZFC magnetization measurements, fig. 6, give a more detailed information on the particle size distribution and interparticle interactions. The temperature T_{max}, at the maximum of the ZFC magnetization curve, is related to the blocking temperature distribution; and the irreversible temperature T_i, where the FC curve starts to deviate from the ZFC curve, is related to the energy barrier distribution in the sample, table 4.

Table 4 Blocking and irreversible temperatures from FC/ZFC

Sample	*T_i K*	*T_{max} K*	*T_b K*	*Mossbauer 80K(Table 1)*
1 PS-12 a 1PS12	195	120	37	sextet
1 PS-10 a 1PS10	35	17	17	Doublet-small sexteto(15%)
3 PS-12 a 3PS12	140	80	34	sextet
3PS-10 a 3PS10	25	15	15	doublet

A larger difference between T_{max} and T_i means a broader particle size distribution. The derivative $\frac{d}{dT}(M_{ZFC} - M_{FC})$ gives the features of the magnetic energy barrier distribution highly correlated to the particle size distribution and also gives the temperature T_b at the maximum of the barrier distribution. In Table 4 it is seen large differences between T_{max} and T_i for the pH 12 samples and

the opposite behavior for the pH 10 samples. With respect to interparticle interactions the pH 12 samples show strong forces and for the pH 10 samples very weak interactions are present. These interactions are also reflected in the increase of T_{max} for pH 12 samples; on the other hand, the flattening of the FC curve at low temperatures is indicating strong interactions between nanoparticle moments, recall the high particle densities from AAS for pH 12 samples [27,28].

It is worth noting that the 80 K Mossbauer spectra showed in fig. 4 was composed of magnetic components in some cases and magnetic-superparamagnetic components for the other cases. A correlation can be drawn with the FC/ZFC magnetic measurement although the samples for the Mossbauer technique were in powder form while for magnetic measurments were gels this may bring small differences in the magnetic behavior of the samples. Sextets were obtained for the samples for which the 80 K temperature (T80) was below T_{max}, i.e. pH 12 samples. For 1PS10 T_{max} and T_i are well below T80 and a doublet should be expected, instead a sextet-doublet line shape appears pointing to the different sample preparation for which the powdering process allows the particle aggregation and further oxidation to maghemite. For 3PS10 a doublet was obtained as expected where the drying process did not affected its properties probably due to the fact that it had the largest amount of polymer covering it.

The interaction of the magnetic particles with the polymer was studied using FTIR, fig. 7, and TGA, fig. 8. table 5 summarizes the FTIR results for the four covered samples.

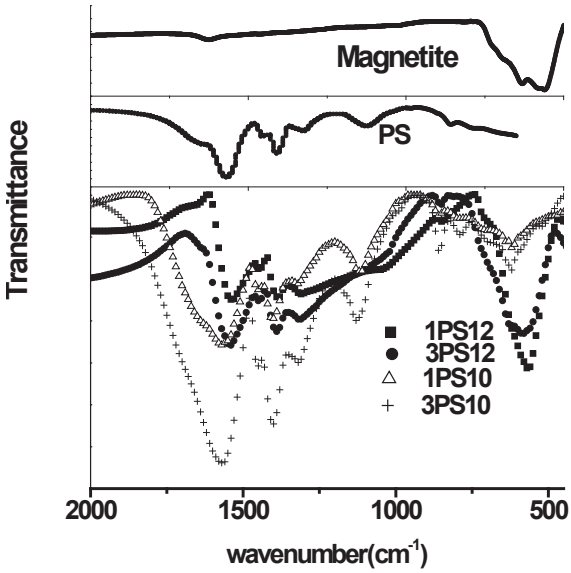

Figure 7 FTIR results for all samples. Pure substances are included as a reference, magnetite and polyacrylate (upper curves). Samples for pH 12 and 10 are presented at the lower curves

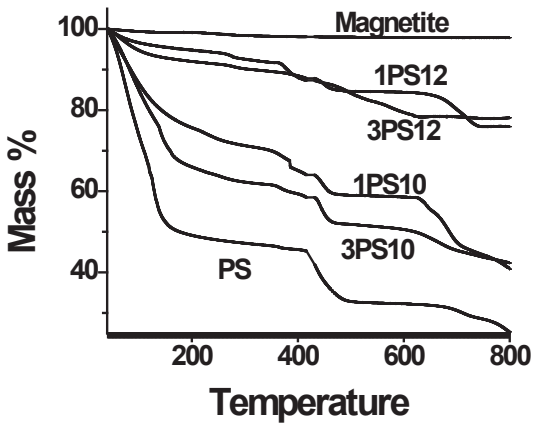

Figure 8 TGA results for polyacrylate samples obtained at pH 12 and 10. Pure magnetite is shown as the upper curve and polyacrylate as the bottom curve

Table 5 FTIR results for all polyacrylate samples

Sample	*Fe_3O_4*	*γFe_2O_3*	*Polyacrylate absorption bands (±4 cm^{-1})*		
			$u_{as}(COO^-)$	*$u_s(COO^-)$*	*Δu*
	434-580	630	1550	1412	138
1 PS-10 a 1PS10		624	1570	1406	164
3 PS-10 a 3PS10		627	1570	1411	159
1 PS-12 a 1PS12	434-584	628	1552	1393	159
3 PS-12 a 1PS12	443-581	625	1541	1390	151

By analyzing the change in the asymmetric stress mode of the polyacrylate carboxylic group COO^- it is noticed a shift in the absorption bands to higher wave number, i.e. from 1550 cm^{-1} in the pure sample to 1570 cm^{-1} for the pH 10 samples, precluding a large interaction with the magnetic nanoparticles surface [29]. The spinel peaks for these samples are less clear due to the large amount of polymer on the surface of the nanoparticles, see results from AAS, for this reason they cannot be determined. The spectra in fig. 7 was normalized in order to enhance the differences in phase composition, for this reason transmittances are not given.

Another route to analyze the interaction particle-polymer is to take the difference between the asymmetric and symmetric stretch absorptions, $\Delta\nu = \nu as(COO^-) - \nu s(COO^-)$, which in this case are larger than in the pure polymer leading preferentially to the formation of a chelating bidentate configurations attached to a single Fe^{3+} on the surface of the particles [18, 30, 31]. The phase composition magnetite/maghemite is also confirmed by FTIR results. TGA gives complementary information about the interaction between the particle surface and the polymer, the results are shown in fig. 8. The pure polyacrylate presents a one step-like curve, from 150-500 C, for which the first sector, 20-150 C, is the loss mass due to physisorbed water, a second sector, 150-400 C, where dehydration and the carboxilate groups dissociation occurs, and the main decomposition occurs in the temperature range 400-500 C.

On the other hand, the covered samples show a two step-like curve which mean that the decomposition takes on at different times due to different polymer layers, with different chemical properties, that surround the magnetic particles. The inner layers decomposed at later times so it can be seen a mayor decomposition in the temperature range 600-750 C. The results also correlate with AAS since samples obtained at pH 12 had a thinner polymer layer but strongly bound to the surface of the particle exhibiting a slower mass loss in such a way that at a temperature of 400 C the mass loss is around 13% while for pH 10 the corresponding quantity is 40%.

Conclusions

The one step coprecipitacion, with surfactant included, produced magnetic nanoparticles covered with significant amount of polymer, especially for the pH 10 samples, as shown by absorption spectroscopy measurements. The magnetic nanoparticles have a magnetite core, and possibly a layer of non-stiochiometric magnetite, surrounded by a maghemite layer and on top of that a surfactant layer, as indicated by Raman, XRD, FTIR, TGA, and magnetic measurements. The TEM images confirm the crystallinity of the nanoparticles, their particle size distribution in the average range of 5-10 nm.

Mössbauer results at 80 K showed line shapes dominated by magnetic relaxation effects with sextets and combinations of sextets and doublets due to the asymmetric lineshapes and very large broadening of sextets. The hyperfine parameters revealed the presence of Fe^{3+}, and small amounts of Fe^{2+} for the dried samples in contrast to gel samples which showed larger content of Fe^{2+}, this indicates a sample oxidation during the drying process. The doublet features dominated the samples obtained at pH 10. Also, the Mössbauer spectra showed effects of interparticle interactions leading to the presence of sextets, especially for pH 12 samples, due to high density of particles embedded in the surfactant which is increased by the drying process. This fact can be understood remembering that the particle size, from XRD and TEM, is in the average range of 5-10 nm ; in this way, it is expected a doublet component at 80 K which is missing.

The interactions of the surfactant with the nanoparticle surface, mainly with the Fe^{3+}, is strong showing at least two surfactant layers, one layer directly over the nanoparticle surface and another layer resting over the inner surfactant layer. This is reflected thorough a step-like structure in the TGA technique. The frequency shifts, intensity and line shape changes in FTIR

confirmed the attachment of the surfactant to the magnetic nanoparticle surface. The main mechanism of binding was the chelating mechanism, due to the fact that both particles and surfactant present a negative charge which leads to repulsion forces between them.

The magnetic behavior was evaluated, in gel form, by moment versus temperature and magnetic field measurements. The nanoparticles showed superparamagnetic behavior at room temperature and ferrimagnetic properties at 5 K. The saturation magnetization presented lower values than reported bulk values and nanosystems prepared by a different route, these occurred due to the presence of a large layer of maghemite. A magnetic diameter was extracted from the initial susceptibility which shows very close values for all samples indicating that a these one-step synthesis conditions, especially large concentrations 1-3%(m/m), the chemical reaction proceeds in a way that the surface properties of the nanoparticles dominate the kinetics. The FC/ZFC plots confirmed the superparamagnetic nature of the iron oxide particles and showed that the distribution of moments was broad for pH 12 samples while it was narrow for pH 10 samples. The magnetic information deduced from Mössbauer spectroscopy confirms the magnetic information extracted from magnetic measurements.

The very close particle size obtained from XRD, TEM, and magnetic measurements gave indication that the particle growth was dominated by the surface properties of the nanoparticles and that the different concentrations and pH did not play a fundamental rol.

The obtained PS-covered nanoparticles may be easily functionalized for biomedicine and bioengineering applications since PS presents charged active sites along the polymeric chain where organic substances can be inmovilized for the applications. Additionaly, PS is biocompatible and biodegradable. Furthermore, the nanoparticles superparamagnetic character makes them appropriate to apply the active susbstance and to control the nanoparticle flux by an external magnetic field.

Acknowledgments

The authors are grateful to Colciencias, Colombian research council, and CODI, Sustainability Program for Solid State Group 2011-2012, Universidad de Antioquia, for financial support.

References

1. A. Gupta, M. Gupta. “Synthesis and Surface Engineering of Iron Oxide Nanoparticles Biomedical Applications”. *Biomaterials.* Vol. 26. 2005. pp. 3995-4021.

2. A. Roca, R. Costo, A. Rebolledo, S. Veintemillas, P. Tartaj, T. Gonzalez, M. Morales, C. Serna. “Progress in the Preparation of Magnetic Nanoparticles for Applications in Biomedicine”. *J. Phys. D: Appl. Phys.* Vol. 42. 2009. pp. 1-11.

3. Y. Zhai, F. Liu, Q. Zhang, G. Gao. “Synthesis of Magnetite Nanoparticle Aqueous Dispersions in an Ionic Liquid Containing Acrylic Acid Anion”. *Colloids and Surfaces A: Physicochem. Eng. Aspects* Vol. 332. 2009. pp. 98-102.

4. G. Herzera, M. Vázquez ,M. Knobel, A. Zhukov, T. Reininger, H. Davies, R. Grossinger, J. Sánchez. “Present and Future Applications of Nanocrystalline Magnetic Materials”. *Journal of Magnetism and Magnetic Materials.* Vol. 294. 2005. pp. 252-266.

5. V. Barbeta, R. Jardim, P. Kiyohara, F. Effenberger, L. Rossi. “Magnetic Properties of Fe_3O_4 Nanoparticles Coated with Oleic and Dodecanoic Acids”. *Journal of Applied Physics.* Vol. 107. Avalaible on: http://arxiv.org/archive/physics. Accessed: April 13, 2010.

6. P. Dallas, V. Georgakilas, D. Niarchos, P. Komninou, T. Kehagias, D. Petridis. “Synthesis, Characterization and Thermal Properties of Polymer/magnetite Nanocomposites”. *Nanotechnology.* Vol. 17. 2006. pp. 2046-2053.

7. L. Harris, J. Goff, A. Carmichael, J. Riffle, J. Harburn, T. Pierre, M. Saunders. “Magnetite Nanoparticle Dispersions Stabilized with Triblock Copolymers”. *Chem. Mater.* Vol. 15. 2003. pp. 1367-1377.

8. K. Nadeem, H. Krenn, T. Traussnig, R. Wurschum, D. Szabo, I. Letofsky. “Effect of Dipolar and Exchange Interactions on Magnetic Blocking of Maghemite

Nanoparticles". *Journal of Magnetism and Magnetic Materials* Vol. 323. 2011. pp. 1998-2004.

9. R. Rebodos, P. Vikesland. "Effects of Oxidation on the Magnetization of Nanoparticulate Magnetite". *Langmuir.* Vol. 26. 2010. pp. 16745-16753.

10. E. Potapova, X. Yang, M. Westerstrand, M. Grahn, A. Holmgren, J. Hedlund. "Interfacial Properties of Natural Magnetite Particles Compared with their synthetic analogue". *Minerals Engineering.* Vol. 36-38. 2012. pp. 187-194.

11. C. Lin, C. Lee, W. Chiu. "Preparation and properties of poly(acrylic acid) oligomer stabilized superparamagnetic ferrofluid". *Journal of Colloid and Interface Science.* Vol. 291. 2005. pp. 411-420.

12. C. Dong. Institute of Physics, Chinese Academy of Sciences. P. O. Box 603, Beijing 100080. Available on: http://www.ccp14.ac.uk/tutorial/powderx/, Accessed: February 2014.

13. JCPDS. *X-ray diffraction data cards of the joint committee on powder diffraction standards*. Software.196 (2001).

14. R. Vandenberghe, E. De Grave, P. De Bakker. "On the Methodology of the Analysis of MössbauerSpectra". *Hyperfine Interactions*. Vol. 83. 1994. pp. 29-49.

15. A. Doriguetto, N. Fernandes, A. Persiano, E. Nunes, J. Greneche, J. Fabris. "Characterization of a Natural Magnetite". *Phys. Chem. Minerals.* Vol. 30. 2003. pp. 249-255.

16. Maria A. G. Soler and Fanyao Qu. "Raman Spectroscopy of Iron Oxide Nanoparticles". C. Kumar (editor). *Raman Spectroscopy for Nanomaterials Characterization*. 1st. ed. Ed. Springer-Verlag. Berlin, Germany. 2012. pp. 379-416.

17. L. Slavov, M. Abrashev, T. Merodiiska, C. Gelev, R. Vandenberghe, I. Markova, I. Nedkov. "Raman Spectroscopy Investigation of Magnetite Nanoparticles in Ferrofluids". *Journal of Magnetism and Magnetic Materials*. Vol. 322. 2010. pp. 1904-1911.

18. F. Nsib, , N. Ayed, Y. Chevalie. "Dispersion of Hematite Suspensions with Sodium Polymethacrylate Dispersants in Alkaline Medium". *Colloids and Surfaces A: Physicochemical and Engineering Aspects.* Vol. 286. 2006. pp. 17-26.

19. F. Tournus, A. Tamion. "Magnetic Susceptibility Curves of a Nanoparticle Assembly II. Simulation and Analysis of ZFC/FC Curves in the case of a magnetic anisotropy energy distribution". *Journal of Magnetism and Magnetic Materials.* Vol. 323. 2011. pp. 1118-1127.

20. A. Novakova, E. Smirnov, T. Gendler. "Magnetic Anisotropy in Fe3O4—PVA Nanocomposites as a Result of Fe3O4-Nanoparticles Chains Formation". *Journal of Magnetism and Magnetic Materials.* Vol. 300. 2006. pp. e354-e358.

21. A. Morales, A. Velásquez, J. Urquijo, E. Baggio. "Synthesis and characterization of Cu^{2+} substituted magnetite". *Hyperfine Interact*. Vol. 203. 2011. pp. 75-84.

22. H. Qi, J. Ye, NanTao, M. Wen, Q. Chen. "Synthesis of Octahedral Magnetite Microcrystals with High Crystallinity and Low Coercive Field". *Journal of Crystal Growth*. Vol. 311. 2009. pp. 394-398.

23. J. Uribe, J. Osorio, C. Barrero, D. Girata, A. Morales, A. Hoffmann. "Physical Properties in thin Films of Iron Oxides". *Microelectronics Journal.* Vol. 39. 2008. pp. 1391-1393.

24. C. Goss. "Saturation Magnetisation, Coercivity and Lattice Parameter Changes in the System Fe3O4-γFe2O3, and their Relationship to Structure". *Physics and Chemistry of Minerals*. Vol. 16. 1988. pp. 164-171.

25. Quantum Design. *Application Note*. Available on: http://www.qdusa.com/sitedocs/appNotes/ppms/1070-207.pdf. Accessed: December 2013.

26. G. Goya. "Handling the Particle Size and Distribution of Fe3O4 Nanoparticles Through Ball Milling". *Solid State Communications*. Vol. 130. 2004. pp. 783-787.

27. E. Lima, E. De Biasi, M. Vásquez, M. Saleta, F. Effenberg, L. Rossi, R. Cohen, H. Rechenberg, R. Zysler. "Surface Effects in the Magnetic properties of crystalline 3 nm ferrite nanoparticles chemically synthesized". *J. Appl. Phys*. Vol. 108. 2010. pp. 103919.

28. D. Parker, F. Ladieu, E. Vincent, G. Mériguet, E. Dubois, V. Dupuis, R. Perzynski. "Experimental Investigation of Superspin Glass Dynamics". *J. Appl. Phys*. Vol. 97. 2005. p. 10A502.

29. A. Zaman, R. Tsuchiya, B. Moudgil. "Adsorption of a Low–Molecular–Weight Polyacrylic Acid on Silica, Alumina, and Kaolin". *Journal of Colloid and Interface Science*. Vol. 256. 2002. pp. 73-78.

30. F. Nsib, N. Ayed, Y. Chevalier. "Comparative study of the Dispersion of Three Oxide Pigments with Sodium Polymethacrylate Dispersants in Alkaline medium". *Progress in Organic Coatings*. Vol. 60. 2007. pp. 267-280.

31. M. McGuire, J. Addai, K. Bremmell. "Spectroscopic Investigation of the Adsorption Mechanisms of Polyacrylamide Polymers onto Iron Oxide Particles". *Journal of Colloid and Interface Science*. Vol. 299. 2006. pp. 547-555.